Heliyon 6 (2020) e05705

Contents lists available at ScienceDirect

Heliyon

journal homepage: www.cell.com/heliyon

Research article

CFD study and experimental validation of low liquid-loading flow assurance in oil and gas transport: studying the effect of fluid properties and operating conditions on flow variables

Miguel Ballesteros Martínez [a,*], Eduardo Pereyra [b], Nicolás Ratkovich [a]

[a] Department of Chemical Engineering, Universidad de los Andes, Cra. 1 #18a-12, Bogota, Colombia
[b] McDougall School of Petroleum Engineering, University of Tulsa, 800 S Tucker Dr, Tulsa, USA

ARTICLE INFO

Keywords:
Chemical engineering
Petroleum engineering
Transport process
Computational fluid dynamics
Petroleum industry
Natural gas
CFD
Low liquid-loading flow
Pipeline transport
Pressure drop
Flow assurance

ABSTRACT

Low liquid-loading flow frequently occurs during the transport of gas products in various industries, such as in the Oil & Gas, the Food, and the Pharmaceutical Industries. Even small amounts of liquid can have a significant effect on the flow conditions inside the pipeline, such as increased pressure loss, pipe wall stresses and corrosion, and liquid holdup along the pipeline. However, most studies that analyze this type of flow only use atmospheric pressures and horizontal 1-in or 2-in pipes, which do not accurately represent the range of operating conditions present in industrial applications. Therefore, this study focused on modeling low liquid-loading flow in medium-sized (6–10 in) pipes, using CFD simulations and experimental data from the University of Tulsa, and then applying it to real operating conditions from a Colombian gas pipeline. An acceptable difference was observed between experimental and CFD data, both for the liquid holdup (18%) and for the pressure drop (12%). Variables like pressure drop and wall shear stress increase with phase velocity, operating pressure, and pipe inclination. Liquid holdup increases with liquid velocity but decreases with all other factors. The relation of flow variables with phase velocities is of particular interest: Doubling the gas velocity decreased holdup 70% and increased pressure drop tenfold. On the other hand, the presence of the liquid phase seems to be more influential on process variables than its exact flowrate; the introduction of the liquid phase to a single-phase gas causes an increase in pressure loss by a factor of three, but doubling the liquid velocity only increases the pressure loss by a further 30%.

1. Introduction

Low liquid-loading flow frequently occurs in many industries, such as in the Oil & Gas, the Food, and the Pharmaceutical Industries. It is colloquially known as wet gas and is defined as any kind of flow with a gas volume fraction larger than 90% (TUV Nel, 2010). Any amount of liquid can significantly affect the pipeline flow conditions (Badie et al., 2000). Even a trace amount of liquid, as little as 0.5%, can increase the pressure drop in a pipeline as much as 30% (Hamersma and Hart, 1987). Wall stresses and corrosion, both of which increase with the presence of a liquid phase or even entrained droplets, must be considered during material selection and wall thickness calculation for any pipeline design, and they may increase capital costs (Karami et al., 2014). The unaccounted presence of a liquid phase can also cause flowrate measuring errors of as much as 60%, which is a grave concern in flow assurance and process control (TUV Nel, 2010).

All of this makes modelling low liquid-loading flow essential for different industries, as well as understanding how fluid properties and operating conditions affect flow assurance variables, i.e, liquid holdup, pressure drop, and wall stresses. This is a particular concern for natural gas transport, from deep wells to downstream facilities, where the large changes in pressure and temperature along the pipeline can cause the condensation of hydrocarbon gases and/or water vapor (Karami et al., 2014).

Nonetheless, most studies found in literature do not model or recreate actual industrial conditions, which usually reach pressures of more than 300 psig and require pipe diameters of up to 10 in (Mucharam, 1990). Three types of studies were found during the literature review: experimental, correlation development, and numerical.

* Corresponding author.
E-mail address: ma.ballesteros641@uniandes.edu.co (M. Ballesteros Martínez).

https://doi.org/10.1016/j.heliyon.2020.e05705
Received 10 September 2020; Received in revised form 15 November 2020; Accepted 8 December 2020

Most experimental studies have only focused on small horizontal pipes (with 1-in [DN 25] to 3-in [DN 80] diameters) at atmospheric conditions (Meng et al., 2001; Olive et al., 2003; Badie et al., 2000). Only in recent years, Rodrigues (2018) and Vuong (2016) have begun testing low liquid-level flows with air-oil mixtures in 6-in [DN 150] pipes at pressures of up to 2.86 MPa, on the TUFFP testing facilities at the University of Tulsa.

Correlation studies, in which 1D mechanistic models are developed to predict flow behavior along the pipe length, have not yet found a model that accurately and reliably predicts flow behavior with low holdups. Additionally, correlations are usually developed only for horizontal low-pressure pipe flow (Banafi et al., 2014; Carraretto et al., 2020).

Numerical studies, in which computational methods are used to model fluid mechanics, are similarly limited. They have only focused on stratified flows of water-air mixtures at atmospheric conditions, and the Computational Fluid Dynamic (CFD) models have not predicted flow conditions accurately with small liquid holdups (Ghorai and Nigam, 2006; Kumar and Ming Bing, 2011; Karami et al., 2014). Even some of the most recent studies, such as Chinello et al.(2019) and López et al. (2016), simulated only liquid holdups over 10% and even then reported errors of up to 30% for flows whose holdups were near this threshold value.

This study focused, therefore, on the development of a reliable, efficient, and accurate computational model for two-phase low liquid-level flow in medium-diameter (6 and 10 in) pipes. We used CFD analysis to model natural gas – condensate flow along a gas pipeline under actual industrial conditions and compared the results with experimental data collected at the University of Tulsa. We then determined the effect of phase velocities, fluid properties, and operating conditions on different flow assurance variables, i.e., pressure drop, flow pattern, liquid holdup, and wall shear stress.

2. Materials and methods

This study was divided into four main steps, each of them focused on one of the project's specific objectives. First, the mesh and physics models were selected to accurately represent the multiphase flow. The experimental conditions from Karami et al. (2014) were used as reference for these initial simulations, because they provided information on possible CFD model configurations and used a short pipe section, which permitted quick model testing, though the simulations presented on their study were limited to air-water mixtures.

Secondly, this CFD model was validated with the experimental data obtained by Vuong (2016). His data was chosen because he used fluids similar to natural gas and condensate, with a large pipe section and a precise measurement of the liquid holdup. He also studied different gas flow rates and pressures, which allowed the analysis of different operating conditions.

Thirdly, the CFD model was applied in a field case study simulating the flow inside several sections from an actual gas pipeline in Colombia, whose operating conditions were detailed by Mucharam (1990). Additional to various pipe inclinations, the effect of the liquid flowrate was also analyzed.

Finally, we simulated a section of the gas pipeline with different liquids to evaluate the effect of the three main fluid properties (i.e., density, viscosity, and surface tension) on flow variables. Since gas density and viscosity at the pressures evaluated are more dependent on operating conditions than on gas composition (Vuong, 2016), only different liquids were analyzed on this step.

2.1. Mesh and physics model

The mesh, multiphase, turbulence, and interface models were selected and refined, in order to ensure that the spatial and time discretization, as well as the modelling equations, would represent the two-phase flow as accurately as possible. Further details of the CFD model selection process can be seen in previous publications (Ballesteros Martínez Miguel et al., 2018); however, the main model testing results are presented in this section along with the model explanation. All initial mesh and Physics model testing simulations were done with an air-water mixture with the following simulating conditions:

2.1.1. Mesh generation

The mesh independence test, which ensures that the mesh configuration does not affect simulation results, involves the analysis of both mesh fineness and the mesh element type. The relation of numerical error and mesh fineness is inversely proportional, as it converges to a stable value once a specific order of magnitude of cell counts is surpassed (Versteeg and Malalasekera, 1995). Thus, the refinement of mesh beyond this point has no purpose, since it does not affect simulation results and only increases computational time. We simulated three different meshes to simulate the low-liquid-level flow: orthogonal, polyhedral, and hexahedral, as shown in Figure 1. Since the stabilization could occur at different cell counts for different mesh types, the three meshes were refined independently.

All simulations results were compared with the experimental value obtained by Karami (2014), using the liquid holdup as a criterion; this liquid holdup was measured in the pipe's outlet to allow as much pipe length as possible for the flow to develop fully. It should be noted that an orthogonal grid is a special kind of hexahedral mesh that is designed to require fewer cells by transitioning from thin layered prismatic cells near the pipe wall to larger hexahedral cells near the pipe core (Hernandez-Perez et al., 2011). Therefore, it only made sense to evaluate it at lower orders of magnitude of cell numbers than those of the other meshes.

The various simulations were then run and plotted against the number of cells for all three different mesh types, as shown in Figure 2. The mesh fineness had little effect on the results with the polyhedral and hexahedral meshes; all the simulation underpredicted the holdup with an average difference of 0.006. On the other hand, orthogonal meshes gave more did not converge and had a larger difference with the experimental value. Based on these results, we selected the hexahedral and the polyhedral meshes as viable options for simulating the system since they gave the same simulation results, though the hexahedral could be used with fewer cells.

Besides the experimental values, the quality of the two possible meshes was also compared, in order to ensure that it would not introduce any significant error into the numerical solution, as shown in Table 1. Various criteria were used as comparison. The cell quality measures the cell geometric distribution and validity; flat cells with faces whose normal vectors point inwards have low-quality indexes. The cell quality average value should be above 0.4, and no cell in the mesh should have a quality of less than 1×10^{-5} (Siemens, 2016), which means that both meshes had good results.

The volume change metric refers to the ratio of any cell with respect to its larger neighbor. The lower the value, the larger the change of sizes between neighboring cells. A value of less than 0.01 can indicate badly meshed regions. Although both meshes have minimum values on the limit of 0.01, the cells with the low volume change metric are all prism cells near the pipe wall, where such drastic changes in cell size are expected. On the other hand, the skewness angle reflects how robustly the diffusion of quantities between the two cells is calculated. Values larger than 90° can result in convergence issues (Siemens, 2016). This means that the polyhedral mesh could have some convergence issues; however, it still predicted the liquid holdup as reliably as the hexahedral mesh, so there was no reason to discard the polyhedral option just based on this criterion.

The hexahedral mesh does present the issue that it suffers more from numerical diffusion when the flow is not aligned with the mesh than a polyhedral grid does. For that reason, in the initial mesh and Physics model testing and in the field case simulations, where flow alignment could not be assured, a polyhedral mesh was used. The hexahedral mesh

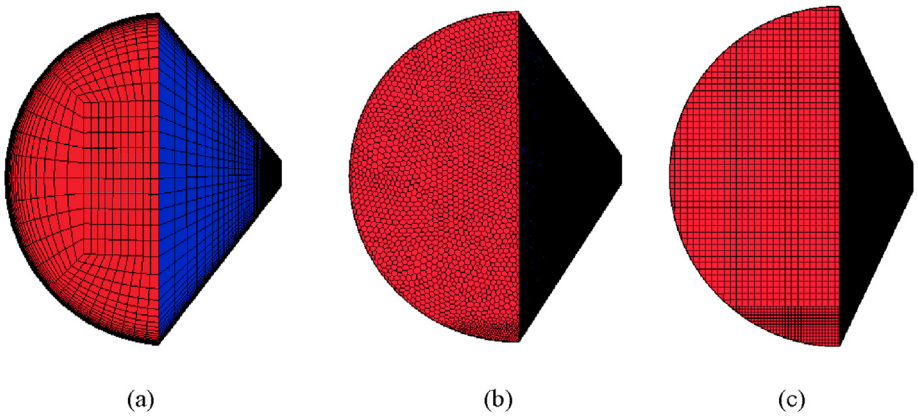

Figure 1. Mesh types considered in the study: (a) orthogonal, (b) polyhedral, and (c) hexahedral.

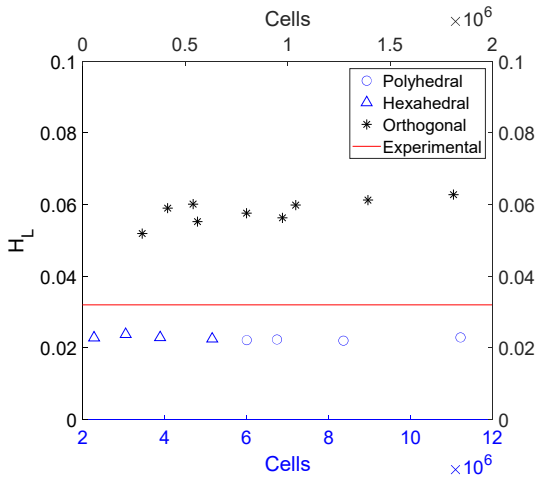

Figure 2. Effect of the number of cells on the holdup (H_L) obtained with three types of meshes: orthogonal (top axis), polyhedral and hexahedral (both on the bottom axis).

was useful for the experimental validation, where the larger pipe section meant more volume had to be meshed.

2.1.2. Boundary conditions

As for boundary and initial conditions, all simulations were configured with the boundaries shown in Figure 3. The phases' velocities were set at the inlet, taking into account the cross-sectional area that each of the phases occupied at the entry. The outlet had a set pressure, which depended on the operating pressure of each simulated case. The pipe wall was set with a no-slip condition. For all simulations, the pipe was initialized as filled with only the gas phase, completely at rest, and with the same pressure as the pressure outlet.

A symmetry plane divided the pipe in half to ease the computational cost. The assumption of symmetry was based on several factors; in most experimental studies found, low liquid level flow in horizontal and inclined pipes developed into segregated or annular flow patterns (Aydin et al., 2014; Vuong, 2016), in which there was no systematic or consistent difference between the left and the right-hand side of the pipe. This means that, though there may be local and temporal differences and perturbations in the flow on each side, the pipe average behavior can still be deduced from modelling just half of it.

This simplification was further supported by the fact that symmetry assumption has been made in various previous CFD studies on multiphase pipe flow to reduce the required computational time (Karami et al., 2014; Daza-Gómez et al., 2019), even with flow patterns far more turbulent and chaotic than a segregated flow. Additionally, after performing the experimental validation, the model was concluded to accurately and reliably predict flow behavior, despite its simplifications.

2.1.3. Multiphase model

The system was simulated using the CFD tool STAR-CCM + v14 (Siemens, Germany), a commercial program with a library of implemented physics models that can be activated and configured to represent different phenomena of interest in the simulated process. The two immiscible phases were modelled as isothermal, since temperature variations were of no interest for this study, and as incompressible, since compressibility can be usually disregarded in flows with a Mach number of less than 0.3 (Anderson, 2011). The Volume Of Fluid (VOF) method

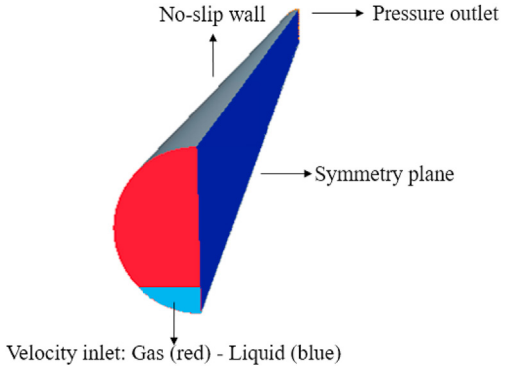

Figure 3. Diagram of the boundary conditions specified for all simulations.

Table 1. Mesh quality parameters.

Variable	Polyhedral mesh	Hexahedral mesh
Average Cell Quality	0.68	0.74
Minimum Cell Quality	0.007	0.003
Minimum Volume Change	0.011	0.011
Maximum Skewness Angle	90	58

was used to simulate the flow. This model assumes that all phases share the same pressure and velocity fields, which means that the two-phase system is modelled as a single-phase fluid, whose volume-averaged physical and transport properties are calculated from the properties of the actual phases.

This means that it requires the introduction of additional differential equations for the volume fraction of the phases. The discretization of these volume fraction equations is done using the High – Resolution Interface Capturing (HRIC) scheme, and the interface is defined as a sharp change from a volume fraction of any phase from 1 to 0; this interface sharpness is affected heavily by space and time discretization, as well as the specific interface models (Waclawczyk and Koronowicz 2008).

$$\frac{d}{dt}\int_V \rho \mathbf{u} dV + \int_A \rho \mathbf{u} \times (\mathbf{u} - \mathbf{u}_g) d\mathbf{A} = -\int_A P\mathbf{I} \cdot d\mathbf{A} + \int_A \boldsymbol{\tau} \cdot d\mathbf{A} + \int_V (\mathbf{f}_r + \mathbf{f}_g + \mathbf{f}_p + \mathbf{f}_u + \mathbf{f}_\omega + \mathbf{f}_L) dV \quad (1)$$

$$\frac{d}{dt}\left(\int_V \alpha_i dV\right) + \int_A \alpha_i (\mathbf{u} - \mathbf{u}_g) d\mathbf{a} = \int_V \left(S_i - \frac{\alpha_i}{\rho_i}\frac{D\rho_i}{Dt}\right) dV + \nabla \cdot (\mathbf{u}_{c_i} \alpha_i (1 - \alpha_i)) \quad (2)$$

A Reynold-Averaged Navier-Stokes equation, like the one shown in Eq. (1), is used to predict the velocity and pressure fields (Siemens, 2016). On the left side of the equation are the terms for transient and convective transport. Meanwhile, the right side of the equation has: the pressure gradient term, the viscous flux term, and the sum of the body forces that can be exerted on the fluid: rotation, gravity, porous media, external forces, vorticity, and electromagnetic fields, respectively.

The conservation equation that describes the transport of the volume fraction of each phase i is shown in Eq. (2). On the left side of the equation are again the terms for the transient and convective transport. On the right side of the equation, the first term takes into account the sources or sinks of the phase, represented in the parameter S_i, and the density variation term. The second term is associated with diffusion and with the sharpening factor, which the users themselves define to improve the resolution of the interface.

Selecting CFD models is usually an act of balancing accuracy and efficiency. Using a single set of transport equations for all phases reduces the computational cost of the model significantly and increases its robustness and stability compared to the Eulerian Multiphase model, which models a separate transport equation for each phase (Guerrero et al., 2017). However, it may also reduce the accuracy of the model. Since the low liquid-loading flow is usually stratified or annular flow (where liquid and gas phases are mostly segregated), and the phases inside a pipe usually flow in the same direction, the VOF model provided the best balance between computational cost and accurate modelling of the pipe flow. It is, after all, the recommended model for such applications (Siemens, 2016).

We modelled the system as a transient process using an implicit method, which uses the information of both the current and the previous time steps. This increases numerical stability and allows for the use of larger time steps than with an explicit method (Pulliam, 1993), which exclusively uses information from the previous time step. The time step used for all simulations was of 0.25 ms, which was calculated using the Courant, Friedrichs, and Lewy (CFL) number. This is a stability criterion used to ensure convergence and stability in the solution of transient problems (Lax, 2013). The logic behind it is that no perturbation in the system should advance through more than a cell in one time step, lest the method begins to diverge.

2.1.4. Turbulence model

As it was a high-Reynolds flow, turbulence and transitional models had to be incorporated. There are three main options usually used in multiphase flow. The first two models, the k –ω and the k – ε models are relatively similar: both are computationally efficient and consist of two balance equations. However, each method has its advantages; the k – ω model can model the viscous regions near the pipe wall more reliably (Menter, 1992b), while k – ε is more robust with respect to inlet condition parameters. Finally, there is the Reynolds Stress Tensor (RST) model, which uses a set of seven equations. This causes the model to be quite computationally expensive, but it can simulate anisotropic and rotational phenomena that cannot be modelled with simpler models (Siemens, 2016).

The three models were compared using the same simulating conditions detailed in Table 2 to check their accuracy; testing revealed that they all predicted similar liquid holdups. However, while both k – ω and k – ε models required a similar simulation times, the RST model required around 150% more time to run. With this in mind, the k – ω model was chosen, because of its computational efficiency and its applicability in near-wall regions without considerable model modifications (Menter, 1992a).

To improve the modeling of the laminar regions near the wall, a transitional model was also implemented, namely, the Gamma Transition model. This model determines the intermittency in each region of the system, i.e., the percentage of time during which the local flow is turbulent, and adjusts specific terms of the turbulence equations accordingly. Gamma Transition has some advantages other options, like a simple Turbulence Suppression model or the Gamma-ReTheta model, that it does not require the calculation of additional inlet variables nor the estimation of transitional regions in the geometry (Siemens, 2016).

$$\frac{d}{dt}\int_V \rho k \, dV + \int_A \rho k (\mathbf{u} - \mathbf{u}_g) \cdot d\mathbf{A} - \int_A (\mu + b_k \mu_t) \nabla k \cdot d\mathbf{A} = \int_V (P_k - \gamma' \rho \beta^* f_{\beta^*} (\omega k - \omega_0 k_0) + S_k) dV \quad (3)$$

$$\frac{d}{dt}\int_V \rho \omega \, dV + \int_A \rho \omega (\mathbf{u} - \mathbf{u}_g) \cdot d\mathbf{A} - \int_A (\mu + b_\omega \mu_t) \nabla \omega \cdot d\mathbf{A} = \int_V (G_\omega - \rho \beta f_\beta (\omega^2 - \omega_0^2) + D_\omega + S_\omega) dV \quad (4)$$

The two-equation system of the chosen turbulence model is shown in Eqs. (3) and (4). In these equations,G_ω represents the specific rate of

Table 2. Simulating conditions for mesh and physics model tests.

Condition	Value
Pipe length	4.57 m~30 L/D
Nominal pipe diameter	6 in [DN 150] SCH 40
Gas superficial velocity	10 m/s
Re_G	1.7×10^5
Liquid superficial velocity	0.02 m/s
Re_L	4.9×10^2
Pressure	0.06 MPa
Temperature	18 °C

dissipation production. G_k is the turbulent production. b_k and b_ω are inverse turbulent Schmidt numbers. S_ω and S_k are user-specified source terms. P_k and γ' are the terms determined by the Gamma Transition model. The remaining unspecified variables refer to parameters specific to the equations.

2.1.5. Interface model

In a real multiphase flow, the immiscibility of the fluids creates a tensile force along the phase interface, which is known as the surface tension force. In the VOF method, this force is modelled using the Continuum Surface Force (CSF) method developed by Brackbill et al., (1992). The CSF method incorporates an additional body force into the momentum transport model shown in Eq. (1) but only for the cells in the interphase region. The additional body force is calculated using Eq. (5). The users can adjust this model by defining certain parameters present in the equations, e.g., the angle factor coefficient that affects the surface curvature term. The CSF model can also be complemented with other models, for example, the Interface Momentum Dissipation model (IMD), which is typically used when there is a significant difference between phase velocities (Siemens, 2016). This model dissipates some of the momentum in the interface by adding an artificial viscosity term to the momentum equations of the cells in the interphase region. This reduces the discontinuity in the velocity field between the phases and may reduce discretization errors at an increased computational cost.

$$\mathbf{f}_{CSF} = \sum_{ij \in Phases} \sigma_{ij} \frac{\alpha_i \rho_i K_j \nabla \alpha_j + \alpha_j \rho_j K_i \nabla \alpha_i}{\frac{1}{2}(\rho_i + \rho_j)} \tag{5}$$

We evaluated different angle factor coefficients using the same simulating conditions detailed in Table 2 to find the value that better predicted the flow behavior. As mentioned before, this factor affects the surface tension force term incorporated in the momentum equation (Siemens, 2016); a higher value helps sharpen the interface, but it may make it artificially align with the mesh. However, all simulations predicted similar liquid holdups, so a default value of 0.2 angle factor was chosen because it provided a well-defined interface.

The inclusion of the IMD model was also tested. Nonetheless, while it did sharpen the interface, as it is shown in Figure 4, it made the simulation prohibitively slow, running at a third of the speed of the other tested configurations. It also did not alter the holdup prediction, so the IMD model was not included in the CFD model used for the rest of the study.

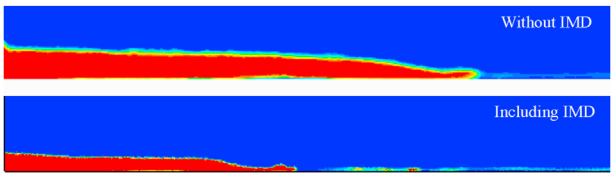

Figure 4. Liquid holdup profile with different model configurations at a simulation time of 0.25 s. The liquid phase is colored red, and the gas phase, blue.

2.1.6. Solver method

The VOF model solves the system by following the numerical procedure summarized in Figure 5. Elahi, Passandideh-Fard, and Javanshir (2015) have an in-depth description of the numerical procedure and the equations. In summary, the user first defines the system, generates the grid and sets the initial conditions. The simulation is then started, and the system is modelled time step by time step, until the desired final physical time is reached.

In each time step, the velocity field is calculated on a two-step process, taking into account: the continuity equation, the Poisson equation for the pressure field, and the Reynolds-Averaged Navier-Stokes (RANS) equation. With these variables, each phase's volume fraction is calculated, and the free surface interface between the phases is constructed. Each time step has its internal iterations, which are terminated when the maximum number is reached, or the equation residuals are low enough.

At the end of each internal iteration, the surface tension force at the interface is calculated and turned into a body force incorporated into the momentum equation, along with the advective and viscous terms. This is taken into account in the next internal iteration. Once the internal iterations are finished, the time step results are displayed, and the simulation jumps to the next time step.

2.2. Experimental validation

The general CFD model was then validated with experimental results obtained at the University of Tulsa (OK, USA) using an Isopar L oil – nitrogen mixture.

2.2.1. Validation design

Three different operating pressures and three gas velocities were simulated to evaluate how these two factors affected the prediction of liquid holdup and pressure drop. This resulted in nine different configurations. The simulating conditions are presented in Table 3.

We adjusted the nitrogen properties for each pressure condition, while the liquid properties were considered constant. The gas density was predicted using the real gas equation and the compressibility factor correlation developed by Span et al., (2000), which is shown in Eq. (7). Meanwhile, the gas viscosity was calculated using the Seibt et al., (2006)

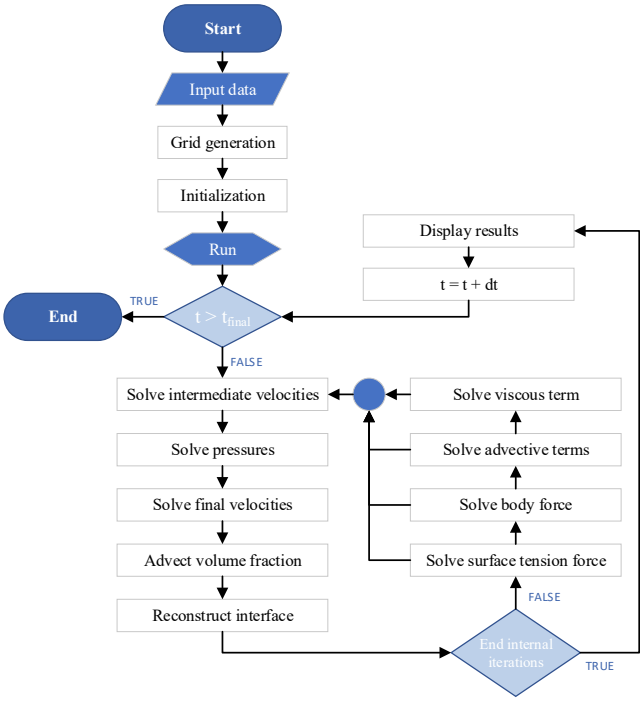

Figure 5. VOF method flowchart.

Table 3. Simulating conditions for experimental validation.

Variable	Level 1	Level 2	Level 3
Pressure	1.48 MPa	2.17 MPa	2.86 MPa
Gas superficial velocity	3 m/s	6 m/s	10 m/s
Pipe length	12.19 m~80 L/D		
Nominal pipe diameter	6 in [DN 150] SCH 40		
Temperature	18 °C		
Liquid superficial velocity	0.04 m/s		

correlation in Eq. (8). These equations depend on the variables δ and τ, which are ratios between either density or temperature, respectively, at simulated and critical conditions. All other variables are correlation parameters.

$$\rho\left[\mathrm{kg}/\mathrm{m}^3\right] = \frac{P[\mathrm{Pa}]\cdot M}{R\cdot T[\mathrm{K}]\cdot Z} \tag{6}$$

$$Z = 1 + \sum_{k=1}^{10} i_k N_k \delta^{i_k} \tau^{-j_k} \tag{7}$$

$$\mu[\mu\mathrm{Pa}\cdot\mathrm{s}] = \sum_{i=0}^{4}\sum_{j=0}^{2} \eta_{ij}\delta^i\tau^{-j} \tag{8}$$

2.2.2. Experimental setup

The data used for experimental validation were collected by Vuong (2016) at the University of Tulsa in the TUFFP, described in the diagram in Figure 6. This facility is designed for experiments with single-phase gas and two-phase gas-oil, and it can recreate pressures of more than 3.45 MPa and pipe inclinations of up to 3° downwards and upwards.

The test section has a pipe length of 85 m, in the middle of which the flow and pressure drop measurement instruments are located, after a pipe length of around 270 times the diameter, in order to ensure that they measure a fully developed flow. The facility is fully suited for the measurement and control of flow variables; it is equipped with temperature and pressure transmitters, differential pressure transducers, quick-closing valves, a wired-mesh sensor for flow pattern analysis, and a Canty visualization system for liquid holdup determination.

The instrumentation installed in the test section are detailed below:

- Pressure transducers: Rosemount 3051- CG with an uncertainty of ±0.15% of the full measurement range.
- Temperature transducers: Rosemount 3144P with an uncertainty of either ±0.25% of the full measurement range or ±0.25 °C, depending on which is the highest.
- Differential pressure transducers: Rosemount 3051-CD with an uncertainty of either ±0.25% of the full measurement range or ±0.25 Pa/m, depending on which is the lowest. Transducers DP1 to DP3 have a range of 747 Pa, while DP4 has a range of 6227 Pa. The differential pressure was calculated by dividing the pressure difference detected in the transducers by the distance between the transducer sensors. Three different distances were used to cover a wide range of pressure drops, as shown in Figure 7.
- Gas and liquid flow meters: The liquid flow was measured with a Micro Motion CMF200 Coriolis meter, with an uncertainty of ±0.05%. As for the gas, two Micro Motion Coriolis meters (CMF100 and CMF300) were used, with an uncertainty of ±0.35%. The CMF100 was used for low gas flow rates, while the CMF300 was used for higher ones.
- Canty Visualization System (CVS): This visual analysis system was based on two HYL 250 Watt light sources (LS) located horizontally opposite of each other on an acrylic section of the pipe, with a Photron Fastcam SA3 high-speed camera (HC) positioned vertically over the pipe, which can record at up to 10000 fps. A diagram of the system is seen in Figure 8(b). The image is then processed to determine the liquid film width, with which the liquid film holdup is calculated.
- Wire Mesh Sensor (WMS): The sensor was composed of a dual mesh system with two 32 × 32 grids separated by a distance of 20 mm. A diagram of the sensor is seen in Figure 8(c). By measuring the electrical capacitance, each grid sensor can determine the type of phase (gas, water, or oil) passing through each of the mesh's squares. With that information, an image of how the liquid and gas phases are distributed can be reconstructed, and the liquid holdup can be calculated. The WMS and the CVS are positioned in the liquid level measurement system shown in Figure 8(a) between two Quick-Closing Valves (QCV).

2.2.3. Uncertainty analysis

Vuong (2016) reported the combined uncertainty of the process variables, with stems from error propagation of the calculations and

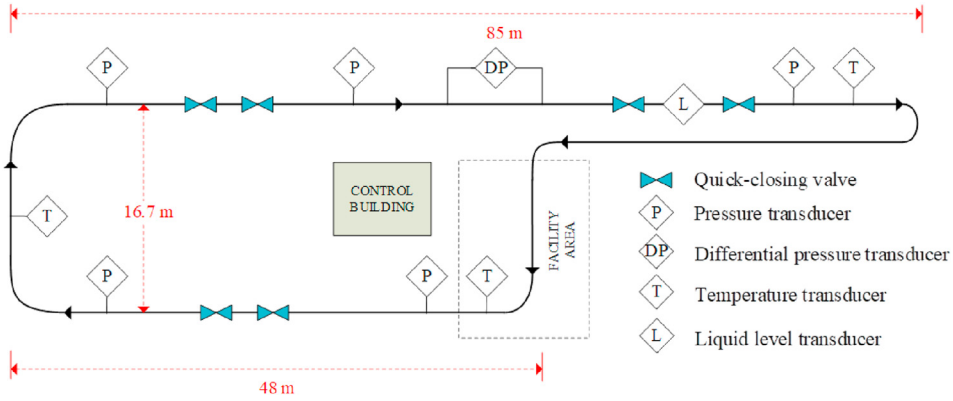

Figure 6. Diagram of the flow facility at the University of Tulsa. Instrumentation and valves are displayed in the diagram, along with test section lengths. The differential-pressure and liquid-level measurement setups are detailed on Figures 7 and 8, respectively.

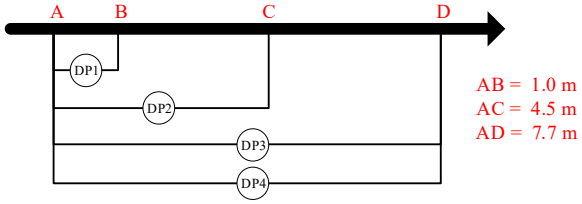

Figure 7. Schematic of the differential pressure measurement setup.

intrinsic instrument uncertainty, as shown in Table 4. It should be noted that the uncertainty of each holdup measuring system depended on the holdup range, and the CVS seemed to be more accurate for low holdup values. Therefore, its values were the ones used for comparison in this study.

2.3. Colombian field case study

After the validation with experimental data, the CFD model was used to analyze the flow conditions (i.e., flow pattern, wall shear stress, pressure drop, and liquid holdup) inside five pipe sections of a Colombian gas pipeline, under real operating conditions, which were taken from a study done by Mucharam (1990).

2.3.1. Operating conditions

The multiphase system behavior was simulated with five pipe sections, which added up to 8 different pipe inclinations, and with three different liquid velocities (one corresponding to a single-phase gas flow). This meant that fifteen different configurations were run in total. All simulating conditions are specified in Table 5.

The condensate density and viscosity were interpolated from experimental data obtained by Khorami et al. (2017). The gas viscosity was obtained from Eq. (9), where the parameters A_1 to A_3 were dependent of the temperature and the molecular weight of the gas, following the equations developed by Heidaryan et al. (2013). On the other hand, the gas density was determined using the real gas equation, where the compressibility factor depended on the reduced pressure and temperature (Dranchuk and Abou-Kassem, 1975). Finally, the interfacial tension coefficient was determined from the gas and condensate compositions, using Eq. (10). The Parachor parameters (P_{chi}) were determined by Fanchi (1990).

Table 4. Simulating conditions for experimental validation.

Variable	Uncertainty
Gas superficial velocity	0.01 m/s
Liquid superficial velocity	0.0004 m/s
Pressure	2.04 Pa
Pressure drop	10 Pa/m
CVS for holdup ≤0.05	0.002
CVS for holdup >0.05	7%
WMS for holdup ≤0.15	0.022 max.
WMS for holdup >0.15	0.015

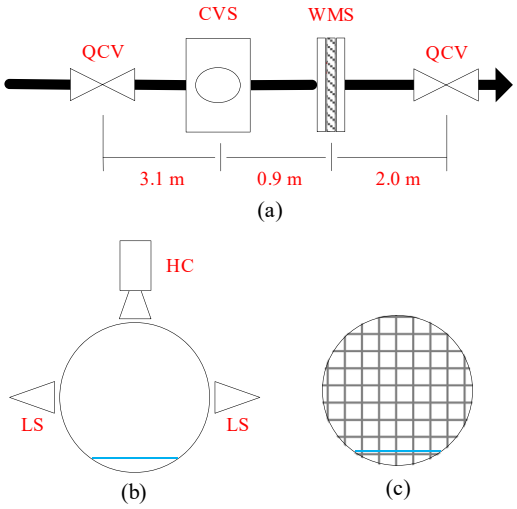

Figure 8. Schematic of the liquid holdup and flow pattern measurement setup.

$$\mu[\mathrm{cP}] = 10^{-4} A_1 \exp\left(A_2 \rho\left[\mathrm{g/cm^3}\right]^{A_3}\right) \tag{9}$$

$$\sigma[\mathrm{dyn/cm}]^{1/4} = \sum_{i=1}^{n} P_{chi}\left(x_i \frac{\rho_L[\mathrm{g/cm^3}]}{M_L} - y_i \frac{\rho_G[\mathrm{g/cm^3}]}{M_G}\right) \tag{10}$$

2.3.2. Pipeline sections

We tested five pipe bend sections from the gas duct, whose height profile can be seen on Figure 9. The sections were selected on their inclination angles to ensure that a wide range of downward and upward angles was covered, as well as different types of bends.

The five pipe sections simulated are shown in Figure 10. All pipe sections had a diameter of 10 in (0.25 m) and a length of 10.2 m. The pipe bend was located in the middle of this length. Following the order shown in the figure, these sections were: two downward pipe sections, a sump, one upward section, and a hump. The bend was set to be 1.5 times the pipe's diameter, following industry standards (SunnySteel, 2011). As some sections shared the same angle of inclination, eight different pipe inclinations were simulated in total, which are summarized in.

2.4. Fluid property analysis

Finally, we studied the effect of liquid properties (i.e., density, viscosity, and surface tension) on the flow variables. All the different

Table 5. Simulating conditions of the field case study.

Variable	Values analyzed			
Pipe inclination	-24.6°	-6.0°	-4.6°	-3.8°
	-3.2°	1.4°	4.4°	11.9°
Pipe length	10.2 m~40 L/D			
Nominal pipe diameter	10 in [DN 250] SCH 40			
Pipe roughness	2.4×10^{-4} m			
Pressure	2.17 MPa			
Temperature	18 °C			
Gas superficial velocity	8.1 m/s			
Liquid superficial velocity	0.0 m/s		0.02 m/s	0.04 m/s

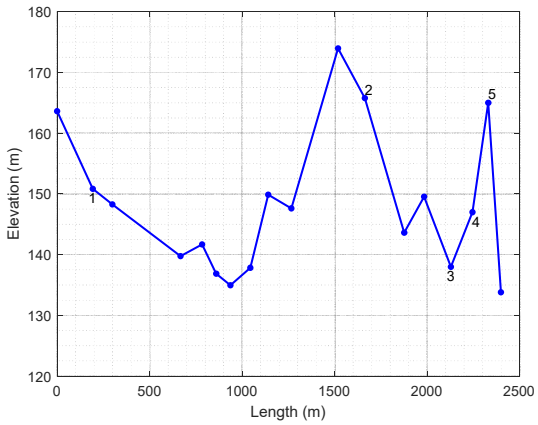

Figure 9. Terrain profile of the gas pipeline taken from Mucharam (1990). The five numbered points represent the pipe bends that were analyzed.

mixtures were simulated following the simulating conditions present in Table 5 and the downward pipe section 1 shown in Figure 10.

2.4.1. Analysis design

The comparison for each property was made selecting two fluids that had similar properties except for the one being evaluated; e.g., Polyoxyethylene Lauryl Ether (PLE) and water have similar densities and viscosities, but the surface tension coefficient of PLE is 60% of that of water (Sadatomi et al., 2010). The comparisons evaluated were:

- Surface tension: PLE and water
- Density: IsoparL oil and water
- Viscosity: IsoparL oil and gas condensate

2.4.2. Fluid properties

The average fluid properties used in the simulations are shown in Table 6. Most of the mixtures were also used in previous steps of the project. Since Vuong (2016) determined that operating conditions varied no more than 1 psig and 1 °C across even a 40-m pipe section, the properties were assumed as constant for each simulation. For the properties of the PLE and air mixture, the values were taken from Sadatomi (2010).

3. Results and discussion

As mentioned, after model selection, the study was developed in three steps: an experimental validation at different pressures and gas superficial velocities, a field case study of different sections of a Colombian gas pipeline with various pipe inclinations and liquid flow rates, and an analysis of the effect of fluid properties on flow variables.

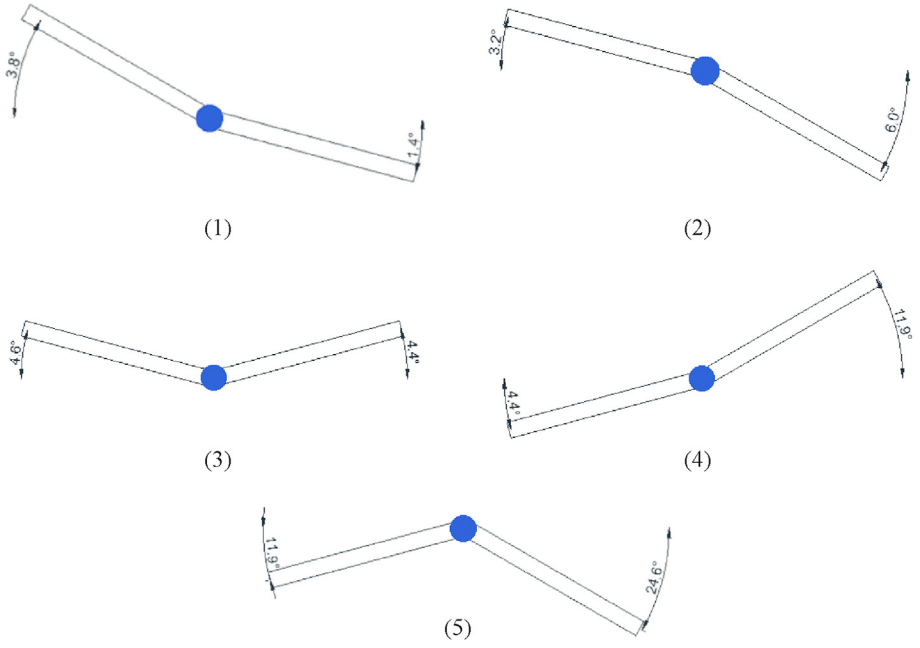

Figure 10. Diagrams of the five pipe configurations simulated, with the respective inclination angles specified. The number of each schematic matches the respective pipe bend in Figure 9.

Table 6. Fluid properties used for the different simulations.

Test fluid	Viscosity (**μPa · s**)	Density (**kg/m^3**)	Surface tension (**N/m**)
Air	18.6	2.05	0.074
Water	889	997.56	
Nitrogen	17.8	16.02	0.024
Isopar L	1300	760	
Natural gas	11.2	18.73	0.054
Condensate	633	752.1	
Air	18.6	2.05	0.042
PLE	922	996	

3.1. Experimental validation

The physics model was validated with the experimental data obtained by Vuong (2016), comparing both liquid holdup and pressure drop. The effect of operating pressure and gas velocity was also analyzed, with both simulation and experimental results.

3.1.1. Experimental comparison

The flow variables were measured in the middle of the pipe section simulated, after allowing enough pipe length for the fully-formed flow to develop. Though the CFD liquid holdup values did not differ too much from the experimental ones, they still were statistically different, with a consistent average underprediction of around 18% (see Figure 11). It should be noted that this error represented a difference of less than 0.02 in the actual value; e.g., for the highest liquid holdup analyzed, the predicted value was 0.057, while the actual experimental value was around 0.076.

A second validation was performed using the pressure drop as a criterion. The difference between experimental and CFD data can be seen in Figure 12. The CFD model tended to underpredict the pressure drop, with an average error of around 12%. Low pressure drops seemed to be more accurately predicted. The smaller average error, in comparison to the liquid holdup, could be caused by the higher order of magnitude of the pressure loss, which makes variations caused by mathematical errors less evident.

Different factors were analyzed as possible causes for the difference between predicted liquid holdups and experimental values. The effect of the liquid entrainment in the gas phase was disregarded as a possible source of error, since the experimental liquid holdup was measured after isolating the pipe section; therefore, the liquid droplets suspended in the gas phase would fall back to the liquid film before the holdup was determined. The difference may be caused by the VOF model's assumptions, as it models both phases as a single phase with volume-averaged fluid properties (Siemens, 2016). The volume-fraction discretization scheme may also cause part of the error.

Karami (2014) reported that lower numerical error could be obtained with a geometric method, at least on water-air mixtures. Geometric methods, unlike compressive methods such as the HRIC scheme that STAR-CCM + uses, reconstruct an explicit representation of the interface based on the VOF volume fraction field (Denner and van Wachem, 2014); they are considered to be more robust and accurate, at the expense of their higher computational cost. However, changing the scheme was not

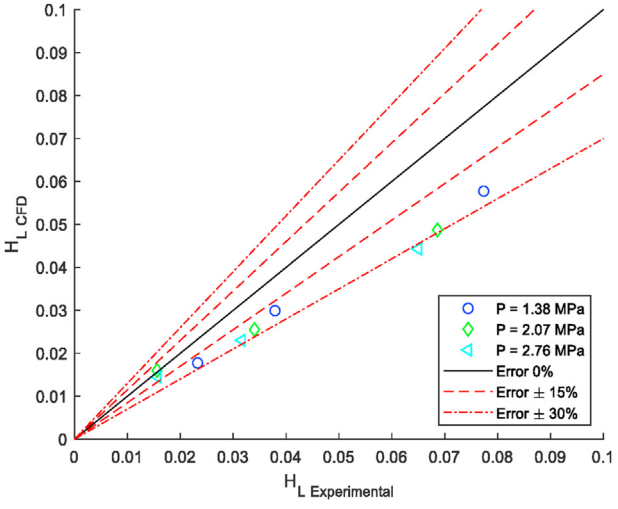

Figure 11. Difference between the experimental and the CFD liquid holdups (H_L).

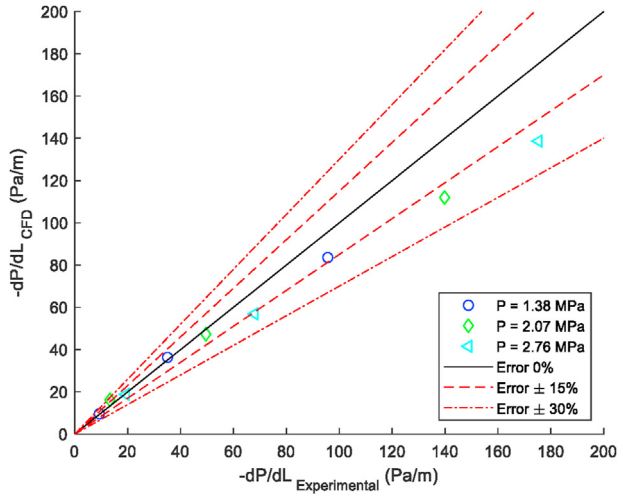

Figure 12. Difference between the experimental and the CFD pressure drop (-dP/dL).

an option with the program used, so this possible solution could not be tested (Siemens, 2016; Karami et al., 2014).

On the other hand, the difference between predicted pressure drop and experimental values may be caused by the assumption of incompressibility and/or the error in the simulated liquid holdup. The holdup's underprediction means that a larger cross-sectional area is left for the gas to flow, which results in smaller gas velocity. As Taitel and Dukler (1976) and Hart et al. (1989) noted, a lower phase velocity is directly related to a smaller frictional pressure drop.

Considering the simplifications assumed by the VOF method, which are related to its computational efficiency, the 20% error for the liquid holdup and 12% for the pressure drop was considered acceptable. This was also based on the fact that in CFD studies, especially of multiphase flow or gas modeling, an error of up to 20% or even 30% is not unusual (Guerrero et al., 2017; Fatima and Chaudhry, 2017; Rivas et al., 2019).

Furthermore, the higher error in the liquid holdup is also due to its low order of magnitude; a relative error of 20% corresponds to a difference of only between 0.01 - 0.02 in the absolute holdup values. Additionally, as it will be discussed in section 3.2.2 of the field case study, even doubling the liquid flow does not have as much of a significant effect on other flow assurance variables (e.g., pressure drop and wall stresses) as the actual presence of a liquid phase, so the underprediction of 20% is not as significant. This implies that the prediction of flow assurance variables and system behavior is nonetheless reliable.

3.1.2. Effect of pressure and gas velocity

Besides comparing experimental and simulated results, an analysis of the effect of gas superficial velocity and operating pressure on liquid holdup was done, which is shown in Figure 13. Both factors seemed to have an opposite impact on the liquid holdup. The increase in gas superficial velocity, from 3 m/s to 10 m/s, caused a decrease of around 70% in experimental and simulated liquid holdups; on the other hand, doubling the pressure from 1.38 to 2.76 MPa reduced holdup by approximately 20% in the CFD results and around 25% in the experimental ones. It should be noted that Vuong (2016) concluded that the effect observed by changes in operating pressure fell within measuring uncertainty, so they could not be determined to be significant.

Even on the simulation results, it can be noticed that gas velocity had a far more significant effect than the operating pressure, which mostly affects the gas density. Nonetheless, the trend observed made sense with the models generally used with the stratified flow, since an increase in either gas velocity or gas density (which is related to the pressure) should increase the interfacial shear stress. This is directly correlated to the

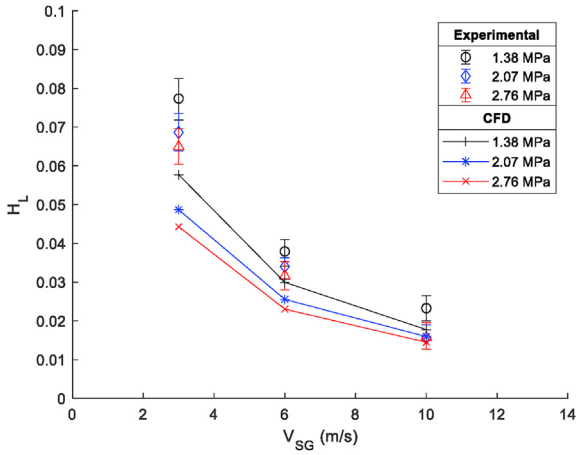

Figure 13. Effect of operating pressure and gas velocities (V_{SG}) on experimental and CFD liquid holdups (H_L).

liquid phase velocity and should, therefore, decrease the liquid holdup (Ghajar and Bhagwat, 2017).

The increase in gas velocity had another secondary effect; it caused the liquid to behave even more laminarly, for it reduced the cross-sectional area available for the oil to flow through. This meant that, while the Reynolds of the gas increased linearly with gas velocity, ranging from 0.4–1.4 $\times$ 10^6, the Reynolds of the liquid phase was reduced by around 50%, from 1.2 to 0.6 $\times$ 10^3, when the gas velocity tripled.

As with the liquid holdup, we also analyzed how the superficial gas velocity and the operating pressure affected the pressure drop along the pipeline. In this case, both factors seemed to affect the response variable directly, as shown in Figure 14. An increase from 200 psi to 400 psi in the operating pressure increased the pressure drop around 73% in the CFD results and 95% in the experimental measurements. The effect of the superficial gas velocity was more significant, as increasing it from 3 m/s to 10 m/s caused the pressure drop to increase around 7.6 times in the CFD and approximately ten times in the experiments.

This increase in the pressure drop meant that, as both gas velocity and operating pressure increased, the pressure loss along the pipe flow became larger. Given that the frictional losses depend directly on gas density (which depends on operating pressure) and gas velocity, the relation observed was expected (Ghajar and Bhagwat, 2017). The effects of operating conditions on the gas viscosity, liquid viscosity, and density,

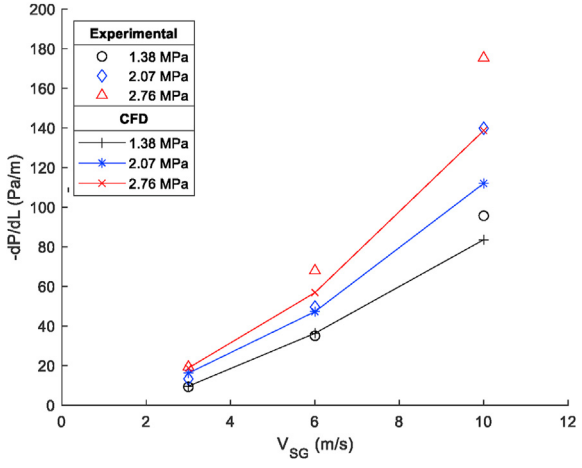

Figure 14. Effect of operating pressure and gas velocities (V_{SG}) on experimental and CFD pressure drop (-dP/dL).

and surface tension were determined to be negligible by Vuong (2016), so variation in their values were not taken into account for this analysis.

3.2. Colombian field case study

Using actual operational conditions from the Colombian gasoduct network, the study analyzed the effect of pipe inclination and liquid velocity on the flow pattern of the phases, the liquid holdup, the pressure drop, and the pipe wall stress. Since each pipe section was composed of two differently inclined pipelines, the flow pattern, the pressure, and the holdup were determined near the end of each inclined pipeline, to ensure: that neither the pipe inlet nor the pipe bend affected the results and that the flow was fully developed. On the other hand, the pipe wall stresses were calculated as the maximum value near each section's pipe bend.

3.2.1. Flow pattern and liquid holdup

The flow pattern observed in the pipe sections depended heavily on their inclination. As expected, upward inclinations prohibited stable, smooth stratified flow from forming (Barnea et al., 1980), favoring a more unsteady wavy flow. Relatively low inclinations, such as the one observed in Figure 15, of around 4.4°, allowed for stratified flow, but with a wavy interface.

The liquid rate effect can also be observed in Figure 15; a higher liquid flow generated a thicker liquid film, and the waves in the interface seemed to be smoother and less affected by the shearing of the gas flow. On the other hand, the thinner liquid film formed with a superficial velocity of 0.02 m/s seemed to be more unsteady, with observable shearing and break-up at the top of the waves. It is important to note that the liquid flow per se was expected to be less turbulent with a lower flowrate since its Reynolds number decreases.

The unsteadiness is probably related to the drag force of the gas phase on the interface. The drag force itself does not change with the liquid velocity since the gas velocity does not change, and the gas Reynolds remains at 3.4 $\times$ 10^6; the higher waviness and shearing is caused then not by a change in force magnitude but a change in relative scale. Since the liquid film is thinner at lower viscosities, the effect of the interface forces becomes more significant concerning the condensate's inertia; therefore, the phase breaks apart and becomes more unstable.

With higher pipe inclinations, no liquid film was able to form, and the phase broke up into droplets dispersed into the gas or small slugs that ran up the bottom of the pipe, as seen in Figure 16. With a more significant liquid flow rate, the slugs in the bottom seemed to form more continuously, indicating a possible annular flow, which is a typical flow pattern with high inclination and gas flow (Shoham, 2005). The system was observed to be very unsteady, with many variations in the flow conditions.

As for the downward inclinations, a smooth, stable stratified flow was achieved, as shown in Figure 17, which allowed for the calculation of the average liquid holdup. These inclinations were measured from pipe sections 1, 2, and the first inclination of pipe section 3.

This liquid holdup was then plotted against the pipe angle, as can be seen in Figure 18. As expected, the liquid holdup seemed to increase with the liquid superficial velocity and decrease with the inclination. Doubling the liquid superficial velocity caused, on average, a 60% increase in the liquid holdup.

The inclination effect seemed to follow a relatively linear relation, and an increase in inclination had a definitive decreasing impact on the holdup. This decrease may probably be related to the fact that, as the flow becomes more inclined, the gravitational influence becomes more significant, accelerating the phase (Taitel and Dukler, 1976).

3.2.2. Pressure drop and pipe wall stress

The analysis of the pressure drop can be seen in Figure 19. These values were obtained from the different inclinations in the five pipe sections simulated; in the cases where there was a repeated inclination

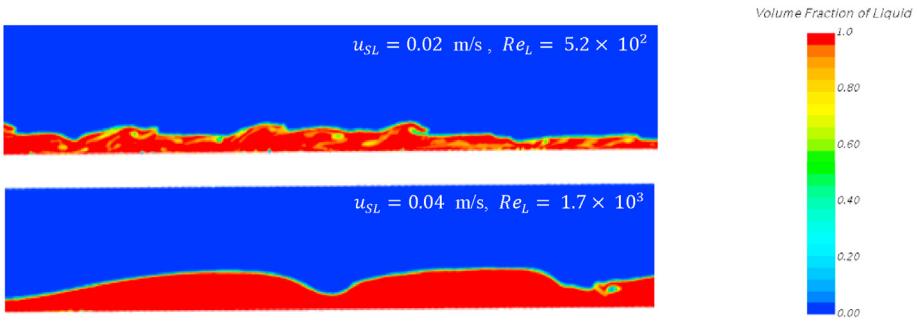

Figure 15. Volume fraction profile for the liquid phase profile (shown in red against the dark blue gas phase), for a natural gas – condensate flow and two liquid velocities flow in a 4.4° upward pipe.

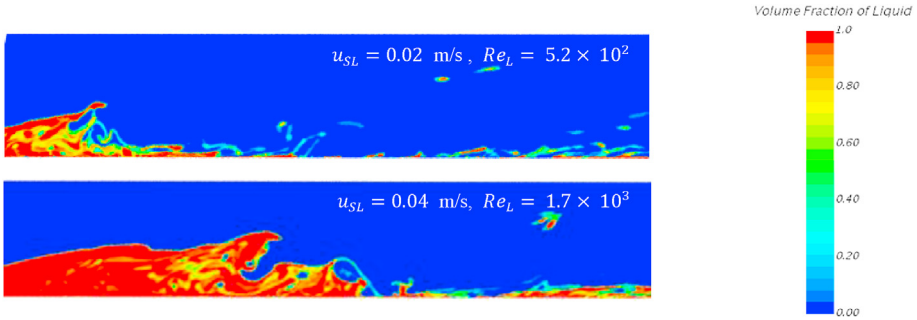

Figure 16. Volume fraction profile for the liquid phase profile (shown in red against the dark blue gas phase), for natural gas – condensate flow in an 11.9° upward pipe with two liquid velocities. All large regions of intermediate colors represent droplets of the dispersed liquid phase.

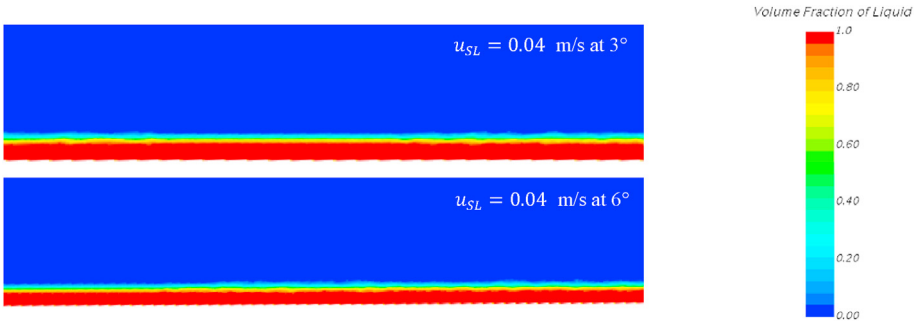

Figure 17. Volume fraction profile for the liquid phase profile (shown in red against the dark blue gas phase), for natural gas – condensate flow in downward pipes.

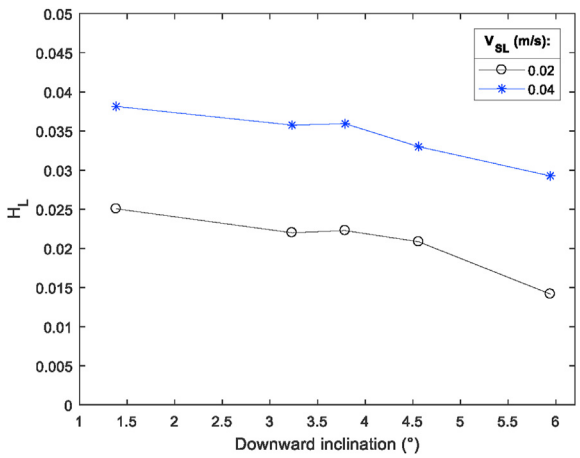

Figure 18. Liquid holdup (H_L) concerning the angle of the downward pipe sections simulated.

(e.g., 4.4° in both pipe sections 3 and 4), the pressure drop plotted was the average value. Two factors were studied: the pipe inclination and the liquid superficial velocity.

The effect of the liquid velocity was relatively straightforward; the higher the velocity, the higher the pressure drop. Given that the pressure drop is directly correlated to the flow rate, such behavior was expected (Wilfred and Bourdelon, 2017). It is interesting to note that the liquid's presence seemed to affect the flow variables more than its actual flow rate, except for particular high upward inclinations, such as the 12° of the hump pipe configurations.

For the rest of the cases, the increase in the pressure drop between the single-phase gas flow and the flow with 0.02 m/s of liquid velocity was about five times bigger than the one that happened when doubling the liquid velocity to 0.04 m/s. The presence of the liquid phase seemed to increase the pressure loss around 2.5 times. Since Hart et al. (1989) reported that a holdup just as little as 0.005 could increase 30% in the pressure drop with respect to the single-phase flow, the observed rise, which occurred with a holdup almost ten times bigger, seemed to be appropriate.

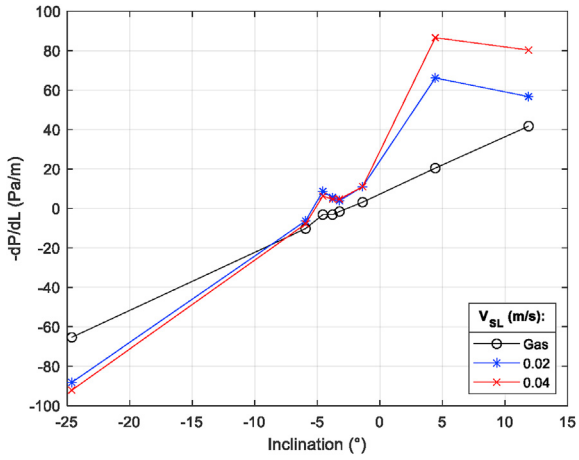

Figure 19. Pressure drop (-dP/dL) versus the angle inclination of the pipe sections simulated, at two different liquid velocities and single-phase gas flow. It should be noted that negative pressure drops mean that pressure rises along the pipeline instead of declining.

The unusual behavior at 12° might have been caused by an annular or dispersed flow pattern, instead of the stratified flow observed with the other inclinations. The fact that the actual liquid velocity, and therefore the holdup, had less effect than the presence of a liquid phase also supports the conclusion that the difference with experimental data was within acceptable limits. With this in mind, the effect of the inclination was more thoroughly studied.

Unlike with horizontal flow, the gravitational force may sometimes cause the pressure to along inclined pipes (Ayala and Adewumi, 2003). The plot in Figure 19 showed that negative inclinations actually reduced the pressure drop or even caused the pressure to increase along the pipeline, as evidenced by the negative pressure drops. On the other hand, positive inclinations increased the pressure drop since it meant that the flow had the gravitational forces working against it.

Both Basha et al. (2014), who worked with high inclinations and medium diameters, and Jeyachandra et al. (2012), who worked with high viscosity oil, identified this same behavior concerning the inclination. However, apart from the single-phase flow, which presented a generally linear behavior, the relation between the pressure drop and the inclination could not be more quantitatively characterized. This was because, in multiphase flow, other factors also play a role in the loss of pressure, such as the phases' flow pattern.

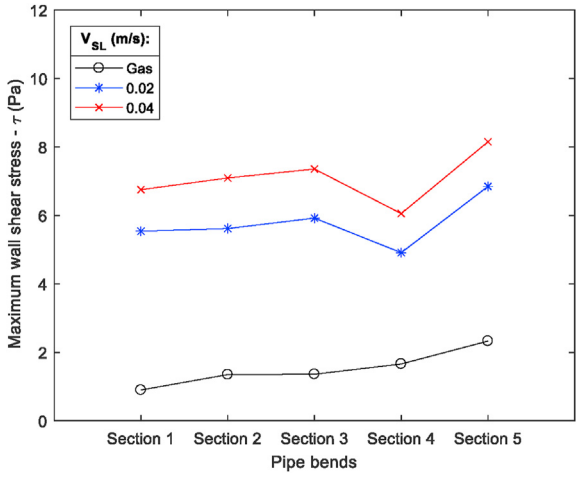

Figure 20. Maximum wall shear stress at the pipe bend for the five-tube sections simulated (which can be seen in Figure 10) for a natural gas – condensate flow on a 10-in pipe, at different liquid velocities and with single-phase flow.

Finally, we also studied how the geometry and the liquid superficial velocity affected the shear stress on the pipe bend wall, as it can be seen in Figure 20. The five different pipe configurations presented relatively similar shear stress values at the bend, except for section 5, which corresponded to the hump configuration. This might have been because it showed a narrower bend angle (140°) than the others, which had around 170°.

As for the liquid rate, the direct relationship between the liquid velocity and the wall stress on the bend was expected since the liquid phase is significantly more viscous than the gas, causing higher strain (Karami et al., 2014). It is interesting to note again that the presence of liquid seemed to have more effect than the actual liquid flow rate; the change in the stress when doubling the liquid velocity is only about 30% of the increase from single-phase to two-phase flow. The effect of the wall stress on flow assurance is, however, still a matter of debate.

The relation between the shear stress and damages in the protective films that prevent corrosion in pipe walls is not well understood yet. Initially, it was believed that after a particular critical value of shearing, the protective film of the pipe could begin to strip, even in single-phase flow (Revie, 2011), but more recent studies have shown that stress alone, even in multiphase flow, is not usually high enough actually to damage it, and more factors have to be at play (Canto Maya, 2015).

Nonetheless, in the case of natural gas transport, which can usually also carry sediments and hydrate crystals, the stress may be related to the erosion-corrosion caused by the impact of the solid particles, since both are concentrated in the areas where there is more shearing between the flow and the pipe wall (Li et al., 2016). Besides that, wall stress is also related to the head loss along the pipeline, affecting flow rate and pressure.

3.3. Fluid properties analysis

The analysis of fluid properties effect on flow behavior was the last set of simulations performed. As mentioned before, the different liquids were simulated on pipe section 1, which has two downward inclinations of 3.8° and 1.4°. For all cases, the pressure drop, the liquid holdup, and the wall stresses were used as criteria for comparison, both statistically and quantitatively.

3.3.1. Effect of mixture surface tension

The study on surface tension was performed using an air/water mixture and an air/PLE mixture because the liquids have similar density and viscosity but a 42% difference in the surface tension coefficient. The pressure drop and the liquid holdup were compared statistically along the pipeline, using a paired-t test. For both variables, the results with both simulations were determined not to be statistically different, so the surface tension seems not to be a significant factor. Since only one average value is obtained for the wall stress at the bend, no statistical analysis could be performed. Table 7 shows the average flow parameters along the pipe section, with both inclination angles.

The values are very similar; this could be because the flow pattern is stratified. The effect of the surface tension has been noticed mostly in bubbly (Sadatomi et al., 2010) or annular (Setyawan and Negeri, 2014) flows, where there are phenomena of the droplet or bubble formation, break-up, coalescence, and impinging.

3.3.2. Liquid density

The comparison was then made between water and the IsoparL oil (see Table 8), which have different densities (the oil is around 24% less dense than water) but similar viscosities. The two liquids did have different surface tension coefficients, but this had already been determined not to be a significant factor.

While increasing density did increase the Reynolds number, which indicated a more turbulent liquid flow, the liquid density was shown to

Table 7. Flow parameters for surface tension analysis.

Flow variable	Water	PLE
Pressure drop at 1° [Pa/m]	15.7	15.4
Pressure drop at 3° [Pa/m]	4.33	4.33
Liquid holdup at 1°	0.038	0.038
Liquid holdup at 3°	0.037	0.037
Maximum wall shear stress at pipe bend [Pa]	9.55	9.46

Table 8. Flow parameters for density analysis.

Flow variable	Water	IsoparL
Pressure drop at 1° [Pa/m]	15.7	15.0
Pressure drop at 3° [Pa/m]	4.33	4.72
Liquid holdup at 1°	0.038	0.038
Liquid holdup at 3°	0.037	0.034
Re_L	1.7×10^3	0.8×10^3
Maximum wall shear stress at pipe bend [Pa]	9.55	8.50

Table 9. Flow parameters for viscosity analysis.

Flow variable	Condensate	IsoparL
Pressure drop at 1° [Pa/m]	11.0	15.0
Pressure drop at 3° [Pa/m]	3.70	4.72
Liquid holdup at 1°	0.038	0.038
Liquid holdup at 3°	0.036	0.034
Re_L	1.6×10^3	0.8×10^3
Maximum wall shear stress at pipe bend [Pa]	6.75	8.50

not have a substantial effect on the liquid holdup and pressure drop, at least on the pipe inclinations analyzed. It may cause a larger difference in more inclined pipes, where gravitational forces play a more prominent role (Ayala and Adewumi, 2003). As for the wall stress, there seems to be a difference in the shear caused by each liquid. Since the frictional forces are related to the phase densities (Ghajar and Bhagwat, 2017), this was expected.

3.3.3. *Liquid viscosity*

The final comparison was made between the gas condensate and the IsoparL oil, which had similar densities, but different viscosities. The condensate has around 50% of the viscosity of the oil. In this case, there was a significant difference in the pressure drop, with the oil having a consistently higher-pressure loss than the condensate. This difference can be noticed in Table 9. On the other hand, there was no statistical difference in the liquid holdup, and the differences are smaller on the average values.

There is a significant difference in the wall stress at the pipe bend, which, along with the higher pressure drop, might be related to the fact that viscosity is directly related to the frictional pressure drop and the shear stress caused by the liquid on the pipe wall (Vuong, 2016; Shoham, 2005). In any case, the effect seemed to be smaller than any impact caused by operating or flow conditions.

4. Conclusions

Low liquid-level flow in natural gas pipelines can be simulated in CFD with reasonable accuracy. The differences observed between experimental and CFD data for the liquid holdup seemed to fall within a range of 20% error. The error for the pressure drop was smaller, of around 12%. This was considered an acceptable error due to the VOF simplifications, the error values typically found in CFD studies, and the small order of magnitude of the liquid holdup.

Phase velocities and operating pressure had the expected effect on flow behavior. The liquid holdup decreased with gas flow rate and operating pressure, while it increased with liquid flowrate. The pressure drop increased with all analyzed variables. The superficial gas velocity (gas flowrate) seemed to be the most significant factor for both flow variables. As for the shear stress on the bend's pipe wall, the highest shearing was observed when the bend angle was narrow, and it increased with phase velocity. However, the relation between wall stress and flow assurance issues, such as erosion or corrosion, is still a matter of debate.

It should be noted that, while all flow parameters increased with liquid velocity, the presence of a liquid phase seemed to be more significant than its flowrate (or superficial velocity). This was noticed both in the pressure drop and in the wall shear stress. The difference in the flow variables between a single-phase gas flow and any two-phase flows was far more significant than the difference caused by doubling the liquid velocity.

As expected, downward inclinations favored stable, smooth stratified flow, decreased the liquid holdup, and caused a pressure rise along the pipe due to gravity influence. Upward inclinations generated unsteady wavy flows or even a possible annular flow; it also increased the pressure drop. The interaction between inclination, turbulence, and phase flowrate was also interesting to note. On horizontal and downward inclinations, where the stratified flow is present, higher gas flowrates decreased the Reynolds of the liquid since they reduced its available flow area. On upward inclinations, increasing the liquid flowrate also seemed to stabilize the liquid phase instead of increasing turbulence and shearing. In this case, it may be related to the fact that a larger flowrate meant a more significant inertial force, which caused the effect of the gas shear on the liquid to be smaller, reducing phase break-up.

Concerning the liquid density, viscosity, and surface tension coefficient, there seemed to be little effect in general compared to the impact of flow or operating conditions, at least with the fluids analyzed. In the case of the density, though no statistical difference could be found; however, there could be a difference in cases with higher inclinations, where the gravitational forces are more significant. Liquid viscosity increased pressure drop and wall shear stress, which agreed with previous studies and correlational models.

Declarations

Author contribution statement

Miguel Ballesteros Martínez: Conceived and designed the experiments; Performed the experiments; Analyzed and interpreted the data; Wrote the paper.

Eduardo Pereyra: Contributed reagents, materials, analysis tools or data.

Nicolás Ratkovich: Conceived and designed the experiments; Contributed reagents, materials, analysis tools or data.

Funding statement

This research did not receive any specific grant from funding agencies in the public, commercial, or not-for-profit sectors.

Data availability statement

Data will be made available on request.

Declaration of interests statement

The authors declare no conflict of interest.

Additional information

No additional information is available for this paper.

Acknowledgements

The authors would like to thank the DSIT and the Vice-Rectory of Research of the Universidad de Los Andes for providing the computing power for the CFD simulations and Duc Huu Vuong the University of Tulsa, for the valuable experimental data.

Earlier versions of this research project were presented at the 10th International Conference on Multiphase Flow - ICMF 2019, and on the 3rd International Conference on Multiphase Flow and Heat Transfer – ICMFHT 2018; the conference proceedings for the latter can be seen on Ballesteros et al. (2018).

References

Anderson, John D., 2011. Fundamentals of Aerodynamics, fifth ed. McGraw Hill, New York.

Ayala, Luis F., Adewumi, Michael A., 2003. Low-liquid loading multiphase flow in natural gas pipelines. J. Energy Resour. Technol. 125 (4), 284.

Aydin, T.B., Torres, C.F., Schleicher, E., Karami, H., Pereyra, E., Sarica, C., 2014. Spatio-temporal features of air-oil interface for stratified-wavy two phase flow in horizontal pipes with a 6-inch diameter. In: 9th North American Conference on Multiphase Technology, pp. 71–83.

Badie, S., Hale, C.P., Lawrence, C.J., Hewitt, G.F., 2000. Pressure gradient and holdup in horizontal two-phase gas-liquid flows with low liquid loading. Int. J. Multiphas. Flow 26 (9), 1525–1543.

Banafi, A., Talaei, M.R., Ghafoori, M.J., 2014. A comprehensive comparison of the performance of several popular models to predict pressure drop in stratified gas-liquid flow with low liquid loading. J. Nat. Gas Sci. Eng. 21, 433–441.

Barnea, Dvora, Shoham, Ovadia, Taitel, Yehuda, Dukler, A.E., 1980. Flow pattern transition for gas-liquid flow in horizontal and inclined pipes. Comparison of experimental data with theory. Int. J. Multiphas. Flow 6 (3), 217–225.

Ballesteros Martínez Miguel, Ángel, Ratkovich, Nicolás, Pereyra, Eduardo, 2018. Analysis of low liquid loading two - phase flow using CFD and experimental data. In: 3rd World Congress on Momentum, Heat and Mass Transfer, 123. Budapest, pp. 1–10. In press.

Basha, M., Shaahid, S.M., Imam, M.M., Ahmad, A., Al-Hadhrami, L.M., 2014. Effect of inclination on the air-water flow in 4-inch pipe. ASME Int. Mech. Eng. Cong. Expos. Proc. 7 (December).

Brackbill, J.U., Kothe, D.B., Zemach, C., 1992. A Continuum method for modeling surface tension. J. Comput. Phys. 100 (2), 335–354.

Canto Maya, Christian M., 2015. Effect of Wall Shear Stress on Corrosion Inhibitor Film Performance. PhD Thesis. Russ College of Engineering and Technology.

Carraretto, Igor Matteo, Colombo, Maria, Pietro, Luigi, Fasani, Damiano, Guilizzoni, Manfredo, Lucchini, Andrea, 2020. Pressure drop and void fraction in horizontal air–water stratified flows with smooth interface at atmospheric pressure. Fluids 5 (3), 101.

Chinello, Gabriele, Ayati, Anis Awal, McGlinchey, Don, Gijsbert, Ooms, Henkes, Ruud, 2019. Comparison of computational fluid dynamics simulations and experiments for stratified air-water flows in pipes. J. Fluid Eng. 141 (5).

Daza-Gómez, Miguel Andrés Mauricio, Pereyra, Eduardo, Ratkovich, Nicolás, 2019. CFD simulation of two-phase gas/non-Newtonian shear-thinning fluid flow in pipes. J. Braz. Soc. Mech. Sci. Eng. 41 (11), 506.

Denner, Fabian, van Wachem, Berend G.M., 2014. Compressive VOF method with skewness correction to capture sharp interfaces on arbitrary meshes. J. Comput. Phys. 279, 127–144.

Dranchuk, P.M., Abou-Kassem, H., 1975. Calculation of Z Factors for natural gases using equations of state. J. Can. Petrol. Technol. 14 (3).

Elahi, R., Passandideh-Fard, M., Javanshir, A., 2015. Simulation of liquid sloshing in 2D containers using the volume of fluid method. Ocean. Eng. 96 (March), 226–244.

Fanchi, John R., 1990. Calculation of parachors for compositional simulation: an update. SPE Reservoir Eng. 5 (3), 433–436.

Fatima, Syeda Firdaus, Chaudhry, Hassam Nasarullah, 2017. Steady-state CFD modelling and experimental analysis of the local microclimate in Dubai (UAE). Sustain. Build 2 (5), 1–12.

Ghajar, Afshin J., Bhagwat, Swanand M., 2017. Gas–liquid flow in ducts. In: Michaelides, Efstathios E., Crowe, Clayton T., Schwarzkopf, John D. (Eds.), Multiphase Flow Handbook. Taylor & Francis Group, Boca Raton, pp. 287–356.

Ghorai, Subhashini, Nigam, K.D.P., 2006. CFD modeling of flow profiles and interfacial phenomena in two-phase flow in pipes. Chem. Eng. Process: Process Intensification 45 (1), 55–65.

Guerrero, Esteban, Muñoz, Felipe, Ratkovich, Nicolás, 2017. Comparison between eulerian and VOF models for two-phase flow assessment in vertical pipes. Ciencia, Tecnología y Futuro 7 (1), 73–84.

Hamersma, P.J., Hart, J., 1987. A pressure drop correlation for gas/liquid flow with A small liquid holdup. Chem. Eng. Sci. 42 (5), 1187–1189.

Hart, J., Hamersma, P.J., Fortuin, J.M.H., 1989. Correlations predicting frictional pressure drop and liquid holdup during horizontal gas-liquid pipe flow with a small liquid holdup. Int. J. Multiphas. Flow 15 (6), 947–964.

Heidaryan, Ehsan, Azad, Jarrahian, 2013. Natural gas viscosity estimation using density based models. Can. J. Chem. Eng. 91 (6), 1183–1189.

Hernandez-Perez, V., Abdulkadir, M., Azzopardi, B.J., 2011. Grid generation issues in the CFD modelling of two-phase flow in a pipe. J. Comput. Multiph. Flows 3 (1), 13–26.

Jeyachandra, Chelinsky, Benin, 2012. Inclination Effects on Flow Characteristics of High Viscosity Oil/Gas Two- Phase Flow, pp. 8–10.

Karami, H., Torres, C.F., Parsi, M., Pereyra, E., Sarica, C., 2014. CFD Simulations of Low Liquid Loading Multiphase Flow in Horizontal Pipelines, 2. American Society of Mechanical Engineers, Fluids Engineering Division (Publication) FEDSM, pp. 1–8.

Khorami, Ahmad, Ali Jafari, Seyed, Mohamadi-Baghmolaei, Mohamad, Azin, Reza, Osfouri, Shahriar, 2017. Density, viscosity, surface tension, and excess properties of DSO and gas condensate mixtures. Appl. Petrochem. Res. 7 (2–4), 119–129.

Kumar, Perumal, Michael, Wong, Ming, Bing, 2011. A CFD study of low pressure wet gas metering using slotted orifice meters. Flow Meas. Instrum. 22 (1), 33–42.

Lax, Peter D., 2013. Stability of Difference Schemes. In: de Moura, Carlos A., Kubrusly, Carlos S. (Eds.), *The Courant–Friedrichs–Lewy (CFL) Condition*. Birkhäuser Boston, Boston, pp. 1–8.

Li, Wei, Pots, B.F.M., Brown, Bruce, Kok, Eng Kee, Nesic, Srdjan, 2016. A direct measurement of wall shear stress in multiphase flow - is it an important parameter in CO2 corrosion of carbon steel pipelines? Corrosion Sci. 110 (April), 35–45.

López, Jorge, Pineda, Hugo, Bello, David, Ratkovich, Nicolás, 2016. Study of liquid–gas two-phase flow in horizontal pipes using high speed filming and computational fluid dynamics. Exp. Therm. Fluid Sci. 76 (September), 126–134.

Meng, Weihong, Chen, Xuanzheng T., Kouba, Gene E., Sarica, Cem, Brill, James P., 2001. Experimental study of low-liquid-loading gas-liquid flow in near-horizontal pipes. SPE Prod. Facil. 240–249.

Menter, F.R., 1992a. Improved two-equation k - w turbulence models for aerodynamic flows. Moffett Field.

Menter, F.R., 1992b. Influence of freestream values on K-omega turbulence model predictions. AIAA J. 30 (6), 1657–1659.

Mucharam, Leksono, 1990. One-Dimensional Compositional Modeling of Gas and Condensate Flow in Pipelines (PhD Dissertation). Pennsylvania State U.

Olive, N.R., Zhang, H.Q., Wang, Q., Redus, C.L., Brill, J.P., 2003. Experimental study of low liquid loading gas-liquid flow in near-horizontal pipes. J. Energy Res. Technol. Transact. ASME 125 (4), 294–298.

Pulliam, Thomas, 1993. Time accuracy and the use of implicit methods. 11th Comput. Fluid Dynam. Conf. Orlando 685–693.

Revie, R. Winston (Ed.), 2011. Uhlig's Corrosion Handbook, third ed. John Wiley & Sons, Inc, Hoboken, NJ, USA.

Rivas, Esther, Luis Santiago, Jose, Lechón, Yolanda, Martín, Fernando, Ariño, Arturo, Pons, Juan José, Miguel Santamaría, Jesús, 2019. CFD modelling of air quality in pamplona city (Spain): assessment, stations spatial representativeness and health impacts valuation. Sci. Total Environ. 649 (1), 1362–1380.

Rodrigues, Hendy, Pereyra, Eduardo, Sarica, Cem, 2018. Pressure effects on low-liquid loading oil-gas flow in slightly upward inclined pipes: flow pattern, pressure gradient and liquid holdup. In: SPE Annual Technical Conference and Exhibition. Society of Petroleum Engineers.

Sadatomi, Michio, Kawahara, Akimaro, Matsuo, Masatoshi, Ishimura, Katsuhiro, 2010. Effects of surface tension on two-phase gas-liquid flows in horizontal small diameter pipes. J. Power Energy Sys. 4 (2), 290–300.

Seibt, D., Vogel, E., Bich, E., Buttig, D., Hassel, E., 2006. Viscosity measurements on nitrogen. J. Chem. Eng. Data 51 (2), 526–533.

Setyawan, Andriyanto, Negeri, Politeknik, 2014. Effects of reduced surface tension on the liquid holdup distribution in horizontal annular two- phase flow. In: IJJSS 2014 : the 6th Indonesia Japan. Yogyakarta.

Shoham, O., 2005. Mechanistic modeling of gas liquid two phase flow in pipes, pp. 240–250.

Siemens, 2016. STAR CCM+ Documentation." NY. http://www.cd-adapco.com/products/star-ccm/documentation.

Span, R., Lemmon, E.W., Jacobsen, R.T., Wagner, W., Yokozeki, A., 2000. A reference equation of state for the thermodynamic properties of nitrogen for temperatures from 63.151 to 1000 K and pressures to 2200 MPa. J. Phys. Chem. Ref. Data 29 (6), 1361–1433.

SunnySteel, 2011. Pipe elbows size data. http://www.sunnysteel.com/elbow-size.php.

Taitel, Y., Dukler, A.E., 1976. A model for predicting flow regime transitions in Horizontal and near horizontal gas-liquid flow. AlChE J. 22 (1), 47–55.

TUV Nel, 2010. Introduction to Wet-Gas Flow Metering. National Measurement System. http://www.tuvnel.com/tuvnel/an_introduction_to_wet-gas_flow_metering/.

Versteeg, H.K., Malalasekera, W., 1995. An Introduction to Computational Fluid Dynamics - the Finite Volume Method. Fluid Flow Handbook. McGraw-Hill.

Vuong, Duc Huu, 2016. Pressure Effects on Two-phase Oil-Gas Low-Liquid-Loading Flow in Horizontal Pipes. PhD Thesis. University of Tulsa.

Waclawczyk, Tomasz, Koronowicz, Tadeusz, 2008. Comparison of CICSAM and HRIC high-resolution schemes for interface capturing. J. Theor. Appl. Mech. 46 (2), 325–345.

Wilfred, Okologume Chinedu, Bourdelon, Marcus Umeleuma, 2017. Comparative analysis of multiphase pressure drop equations. Int. J. Eng. Modern Technol. 3 (4), 1–17.